All-optical generation of quantum entangled states with strictly constrained ultrafast laser pulses

Yu Guo,[1,2] Xiaobing Luo,[3] Shan Ma,[4] and Chuan-Cun Shu[1,*]

[1]*Hunan Key Laboratory of Super-Microstructure and Ultrafast Process, School of Physics and Electronics, Central South University, Changsha 410083, China*

[2]*Hunan Provincial Key Laboratory of Flexible Electronic Materials Genome Engineering, School of Physics and Electronic Science, Changsha University of Science and Technology, Changsha 410114, China*

[3]*Institute of Atomic, Molecular Physics & Functional Materials, Department of Physics, Jinggangshan University, Ji'an 343009, China*

[4]*School of Automation, Central South University, Changsha 410083, China*

(Received 8 May 2019; published 12 August 2019)

We present a quantum optimal control theory study combined with theoretical analysis to determine a pulsed laser field, capable of generating a maximally entangled state in two trapped two-level atoms. By expanding the time-dependent unitary operator to the first leading term of Magnus expansion, we reexamine the pulse area theorem for the trapped atoms driven by an arbitrarily temporary field. Due to the dipole-dipole interaction blockade, we find that the two trapped atoms described by a three-level ladder system can be reduced into an equivalent two-level model by using narrow-bandwidth pulses, leading to an analytical solution for generating the maximally entangled state. We also solve a highly constrained optimization problem to search for optimal laser pulses with broad bandwidths. A zero pulse-area constraint is employed to remove the dc offset of the optimized laser pulses, and a fixed fluence limitation combined with a constant pulse-area constraint at the resonant frequency of the equivalent two-level system are utilized to restrict the unitary evolution of quantum systems by the first leading term of Magnus expansion. This work provides a potentially useful approach to find all-optical control schemes for generating the maximally entangled state by using ultrafast laser pulses while satisfying multiple strict limitations.

DOI: 10.1103/PhysRevA.100.023409

I. INTRODUCTION

Proposed by Richard Feynman decades ago [1], quantum computers are seen as a successor of contemporary computers, in which quantum bits (qubits) can represent far more information than the classical binary bits, massively increasing computing speed and capacity. To build real-world quantum computers [2], a number of quantum schemes and technologies have been demonstrated in superconducting circuits [3,4], quantum dots [5], nuclear spin [6], trapped ions [7,8], and neutral atoms [9,10] to search for candidates of qubits defined by two energy levels of atoms or ions [11]. When two qubits are separated in space and are coupled through dipole-dipole interactions, a basic concept in field is to create quantum entanglement [12–16] in the context of composite qubits with the help of photons [17–21].

Since perturbations, noise, and other environmental effects lead to decoherence, a series of closely related schemes have been proposed for speeding up the generation of entangled states beyond the adiabatic approaches [22–24]. The use of ultrafast laser pulses is able to operate qubits on extremely short timescales before quantum decoherence plays roles [25,26], which could eventually lead to a breakthrough in quantum computing. For the two-atom entanglement, recent ultrafast quantum control experiment has obtained the entangled state with the fidelity of $(76 \pm 1)\%$ in atomic ion qubits [27]. Alternatively, neutral atoms are providing an emerging platform for qubits with attractive advantages [28]. On the one hand, they can be extremely well isolated from surrounding environmental noise and can also be finely controlled using optical traps (or tweezers). On the other hand, they are all identical and can be prepared in well-defined initial states by using optical pumping techniques. Recent theoretical and experimental works have demonstrated that a single-excitation Bell state can be obtained between two neutral atoms [29,30]. A mechanism referred to Rydberg blockade is involved through long-range dipole-dipole interactions with negligible spin-orbit and exchange effects [31], which due to large dipole moments are still large enough to shift the double excitation of the system out of resonance, leading to the inhibition of the excitation of ground-state atoms to the Rydberg state by the presence of a nearby Rydberg atom.

This work will take the advantages of both neutral atoms and ultrafast quantum control, and examine how a pulsed laser field can be designed to generate the maximally entangled states in two trapped two-level atoms. We consider the dipole-dipole interaction in a resonant coupling approach, i.e., the Ising model for describing the exchange interaction. By deriving a pulse area theorem for the two trapped two-level atoms in the presence of an arbitrarily temporary field, we find that the double-excitation state can be energetically forbidden by using narrow-bandwidth laser pulses, leading to an equivalent two-level system for generating the maximally entangled state. However, it remains a challenging task to design the ultrafast laser pulses with broad bandwidths by

*cc.shu@csu.edu.cn

using the pulse area theorem. We thus attempt to access the solutions with the help of quantum optimal control theory (QOCT).

Building on pioneering efforts, QOCT has demonstrated wide success in a variety of quantum systems to determine the temporal shape of an applied external field [32–36]. The optimal solutions are always accessible in the case of free constraints, though they are usually complex for insights. In practice, there are always restrictions on the applied fields, which may significantly limit the searching space to access globally optimal solutions [37–45]. In this work, we will demonstrate the fact that the constraints can be utilized to find the temporal shapes of the optimized fields in an all-optical control approach, consisting of two time-delayed laser pulses. We employ a recently developed QOCT method [44] to search for an ultrafast laser pulse, capable of generating the maximally entangled state while satisfying multiple strict limitations. First, the dc offset of the fields vanishes for all-optical control. Second, we restrict the fluence of the optimized fields to be the same as the initial input, and therefore no further energy consuming is required. In addition, the pulse area of the optimized fields is fixed at the resonant frequency between the ground state and the maximally entangled state, which provides access to gain insights into the breakdown of the derived pulse area theorem.

The paper is organized as follows. In Sec. II, we derive a pulse area theorem, and then we review briefly the optimization algorithm we use. We present the results of numerical simulation in Sec. III. We conclude our paper in the final section.

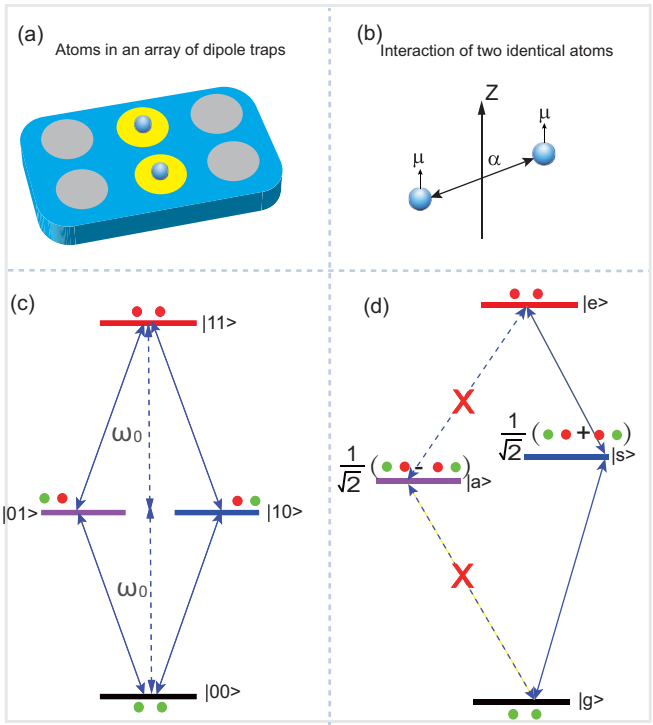

FIG. 1. (a) Schematic illustration of the theoretical model consisting of two ultracold neutral atoms trapped in an array of optical traps, and (b) diagrammatic representation of such a system in space. Collective states of the two atoms (c) in the absence of and (d) in the presence of the dipole-dipole interaction.

II. THEORETICAL METHODS

We consider a system of two identical two-level atoms in controlled arrays of optical dipole traps separated by a distance d, as shown in Figs. 1(a) and 1(b). Each of the traps contains an individual atom that consists of two levels $|0\rangle$ and $|1\rangle$ with transition frequency ω_0 and dipole moment μ along the same direction, which has an angle α with the line connecting the two atoms. We focus on the system interacting through Ising coupling and the field-free Hamiltonian of the system reads ($\hbar = 1$)

$$H_0 = \frac{\omega_0}{2}\sum_{i=1}^{2} S_i^z + V_{dd}\sum_{i\neq j=1}^{2} S_i^+ S_j^-, \tag{1}$$

where S_i^+, S_i^-, and S_i^z denote the raising, lowering, and energy difference operators of the ith atoms, and the dipole-dipole potential between the atoms V_{dd} takes the form,

$$V_{dd} = \frac{3}{4}\gamma\left\{\left(1-3\cos^2\alpha\right)\left[\frac{\sin(kd)}{(kd)^2}+\frac{\cos(kd)}{(kd)^3}\right] - \left(1-\cos^2\alpha\right)\frac{\cos(kd)}{kd}\right\}, \tag{2}$$

with $\gamma = \frac{\omega_0^3\mu^2}{3\pi\epsilon_0 c^3}$ and $k = \omega_0/c$ [46].

In the absence of dipole-dipole coupling, i.e., $V_{dd} = 0$, the basis states of two atoms can be written by four product states $|00\rangle$, $|01\rangle$, $|10\rangle$, and $|11\rangle$ with eigenvalues $E_{00} = -\hbar\omega_0$, $E_{01} = 0$, $E_{10} = 0$, and $E_{11} = \hbar\omega_0$, as sketched in Fig. 1(c). In the presence of dipole-dipole coupling, i.e., $V_{dd} \neq 0$, the perturbed eigenvalues of H_0 can be given by $E_g = -\omega_0$, $E_a = -V_{dd}$, $E_s = V_{dd}$, and $E_e = \omega_0$, and the corresponding eigenstates can be represented by the basis of Dicke sates $|g\rangle = |00\rangle$, $|a\rangle = (|01\rangle - |10\rangle)/\sqrt{2}$, $|s\rangle = (|01\rangle + |10\rangle)/\sqrt{2}$, and $|e\rangle = |11\rangle$, as shown in Fig. 1(d). The symmetric state $|s\rangle$ and antisymmetric state $|a\rangle$ are known as the maximally entangled two-qubit Bell states. When such a pair of trapped atoms are simultaneously interacted with a time-dependent electric field $\mathcal{E}(t)$ along the direction of the dipole moment, the unitary evolution of the system obeys the equation,

$$i\hbar\frac{\partial U(t,t_0)}{\partial t} = \left[H_0 - \mu\mathcal{E}(t)\sum_{j=1}^{2}(S_j^+ + S_j^-)\right]U(t,t_0), \tag{3}$$

with $U(t_0,t_0) \equiv \mathbb{I}$. We consider the system initially in state $|g\rangle$ and thus the time-dependent probability of three states can be obtained by $P_i(t) = \langle g|U^\dagger(t,t_0)|i\rangle\langle i|U(t,t_0)|g\rangle$ with $i = g, s$, and e. This work aims to design the temporal shapes of control fields $\mathcal{E}(t)$ to drive the quantum system from the initial state $|g\rangle$ at $t = t_0$ to the Maximally entangled Bell state $|s\rangle$ at $t = t_f$.

In the basis of Dicke states, the antisymmetric state $|a\rangle$ is decoupled from the states $|g\rangle$, $|s\rangle$ and $|e\rangle$, and therefore the system is reduced into a three-level system with the

Hamiltonian (see the proof in Refs. [47,48]),

$$H^d(t) = \sum_{p=g,s,e} |p\rangle E_p \langle p| - \mu^d \mathcal{E}(t) \left(\sum_{p\neq q}^{g,s} |p\rangle\langle q| + \sum_{p\neq q}^{s,e} |p\rangle\langle q| \right), \tag{4}$$

which can be written in the interaction picture without using RWA by

$$H_c^d(t) = -\mu^d \mathcal{E}(t) \left[\sum_{p\neq q}^{g,s} |p\rangle\langle q| e^{i\omega_{pq}t} + \sum_{p\neq q}^{s,e} |p\rangle\langle q| e^{i\omega_{pq}t} \right], \tag{5}$$

with $\omega_{pq} = (E_p - E_q)$ and $\mu^d = \sqrt{2}\mu$. We start with the derivation of an analytic solution for such a three-level system interacting with an arbitrarily time-dependent control field $\mathcal{E}(t)$. We employ Magnus expansion to describe the time-dependent unitary operator [49,50],

$$U(t, t_0) = \exp\left[\sum_{n=1}^{\infty} S^{(n)}(t) \right], \tag{6}$$

where the first leading term can be written as $S^{(1)}(t) = iA(t)$ with

$$A(t) = -\int_{t_0}^{t} dt_1 H_c^d(t_1) \tag{7}$$

for describing the first-order interactions between states. The time-dependent unitary operator with the first leading term $U^{(1)}(t, t_0) = \exp[iA(t)]$ can be described as [51]

$$U^{(1)}(t, t_0) = e^{iE_0(t)} |\psi_0\rangle\langle\psi_0| + e^{iE_+(t)} |\psi_+\rangle\langle\psi_+| + e^{iE_-(t)} |\psi_-\rangle\langle\psi_-|, \tag{8}$$

where $E_0(t) = 0, E_-(t) = -\theta(t)$, and $E_+(t) = \theta(t)$ are the eigenvalues of $A(t)$, and the corresponding eigenstates are

$$|\psi_0\rangle = \frac{|\theta_{sg}(t)|}{\theta(t)} \left(-\frac{\theta_{es}^*(t)}{\theta_{sg}(t)} |g\rangle + |e\rangle \right), \tag{9}$$

$$|\psi_-\rangle = \frac{1}{\sqrt{2}} \frac{|\theta_{es}(t)|}{\theta(t)} \left(\frac{\theta_{sg}^*(t)}{\theta_{es}(t)} |g\rangle - \frac{\theta(t)}{\theta_{es}(t)} |s\rangle + |e\rangle \right), \tag{10}$$

$$|\psi_+\rangle = \frac{1}{\sqrt{2}} \frac{|\theta_{es}(t)|}{\theta(t)} \left(\frac{\theta_{sg}^*(t)}{\theta_{es}(t)} |g\rangle + \frac{\theta(t)}{\theta_{es}(t)} |s\rangle + |e\rangle \right), \tag{11}$$

with $\theta_{sg}(t) = \mu^d \int_{t_0}^{t} dt' \mathcal{E}(t') e^{i\omega_{sg}t'}$, $\theta_{es}(t) = \mu^d \int_{t_0}^{t} dt' \mathcal{E}(t') e^{i\omega_{es}t'}$, and $\theta(t) = \sqrt{|\theta_{sg}(t)|^2 + |\theta_{es}(t)|^2}$.

We can obtain an analytic solution $|\psi^{(1)}(t)\rangle = U^{(1)}(t, t_0)|g\rangle$ by applying the first-order term $S^{(1)}(t)$ to the time-dependent unitary operator, i.e.,

$$|\psi^{(1)}(t)\rangle = \frac{|\theta_{es}(t)|^2 + |\theta_{sg}(t)|^2 \cos\theta(t)}{\theta^2(t)} |g\rangle + \frac{i\theta_{sg}(t) \sin\theta(t)}{\theta(t)} |s\rangle + \frac{\theta_{sg}(t)\theta_{es}(t)}{\theta^2(t)} [\cos\theta(t) - 1] |e\rangle, \tag{12}$$

for a three-level ladder system, which in form is similar to the solution of a three-level Λ system with a conjugate of $\theta_{es}(t)$, but is different from the solution of a three-level V system; see details in Ref. [50]. The solution by Eq. (12) combined with that for the three-level Λ and V systems in Ref. [50] establishes a full pulse area theorem for all three types of three-level systems, whereas the forms of the time-dependent wave function are dependent on the initial state $|\psi(t_0)$.

It can be seen from Eq. (12) that the Maximally entangled Bell state $|s\rangle$ can be obtained if the control field $\mathcal{E}(t)$ satisfies two conditions $\theta_{sg}(t_f) = \pi/2$ and $\theta_{es}(t_f) = 0$. Since the state $|s\rangle$ is shifted out of resonance of individual atoms at ω_0, a long laser pulse centered at $\omega_{sg} = \omega_0 + V_{dd}$ with a narrow bandwidth of $\Delta\omega < V_{dd}$ can be utilized to resonantly excite state $|s\rangle$ while blocking state $|e\rangle$, leading to a coherent superposition of the ground state $|g\rangle$ and the Bell state $|s\rangle$, i.e., $\cos\theta(t)|g\rangle + i\sin\theta(t)|s\rangle$.

The use of ultrashort pulses with broad bandwidths of $\Delta\omega > V_{dd}$ will break the above two-level model, giving rise to a challenge to obtain analytical solutions. To that end, we employ a QOCT method developed recently in Ref. [42] to solve this raised problem to search for optimal control fields, which are able to generate the maximally entangled Bell state while simultaneously satisfying multiple equality constraints $h_m[\mathcal{E}(\cdot)] = C_m$ for $m = 1, ..., M$. By introducing a dummy variable x, the optimization problem is demonstrated as follows:

$$\frac{dP_s(t_f)}{dx} = \int_{t_0}^{t_f} \frac{\delta P_s(t_f)}{\delta \mathcal{E}(x,t)} \frac{\partial \mathcal{E}(x,t)}{\partial x} dt \geqslant 0, \tag{13}$$

$$\frac{dh_m[\mathcal{E}(x,\cdot)]}{dx} = \int_{t_0}^{t_f} \frac{\partial h_m[\mathcal{E}(x,\cdot)]}{\partial \mathcal{E}(x,t)} \frac{\partial \mathcal{E}(x,t)}{\partial x} dt = 0. \tag{14}$$

A solution to simultaneously satisfying Eqs. (13) and (14) can be obtained by considering

$$\frac{\partial \mathcal{E}(x,t)}{\partial x} = S(t) \sum_{j=0}^{M} [\Gamma^{-1}]_{0j} c_j(x,t), \tag{15}$$

with $c_0(x,t) = \delta P_s(x)/\delta\mathcal{E}(x,t)$, and $c_m(x,t) = \partial h_m/\partial\mathcal{E}(x,t)$ for $m = 1, ..., M$. In Eq. (15), a smooth envelope function $S(t)$ is used to restrict the variation of $\mathcal{E}(x,t)$ with respect to dummy variable x, and the matrix Γ is composed of the elements $\Gamma_{jj'} = \int_{t_0}^{t_f} dt c_j(x,t) S(t) c_{j'}(x,t)$. Note that this QOCT method can strictly fix multiple constraints. In this work, we impose three equality constraints on the search directions with $h_1 = \int_{t_0}^{t_f} \mathcal{E}(x,t)dt$, $h_2 = \int_{t_0}^{t_f} \mathcal{E}^2(x,t)dt$ and $h_3 = \int_{t_0}^{t_f} \mathcal{E}(x,t)\cos(\omega_{sg}t)dt$. The first constraint h_1 at zero can be used to vanish the dc component for all-optical control, the second one h_2 keeps the total energy unchanged, and the third one h_3 can be used to restrict the optimized fields to satisfy a condition of $\theta_{sg}(t_f) = \pi/2$, so that the first leading term $S^1(t)$ plays dominant roles in achieving the control target. We therefore get $c_1(x,t) = 1$, $c_2(x,t) = 2\mathcal{E}(x,t)$, $c_3(x,t) = \cos\omega_{sg}t$. We then solve Eq. (15) from an initial guess $\mathcal{E}(x_0,t)$ to obtain the optimized laser field $\mathcal{E}(x_{\max},t)$ in an iterative approach. The details for this optimization method and its extensions can be found in our previous papers [42–45]. Note that this work extends the application of the optimization algorithm of Eq. (15) to include three equality constraints, which is different from that examined in Ref. [42] by only considering the first two constraints. The application of the algorithm for the system combined with the results obtained in this work is also different from that in Ref. [42].

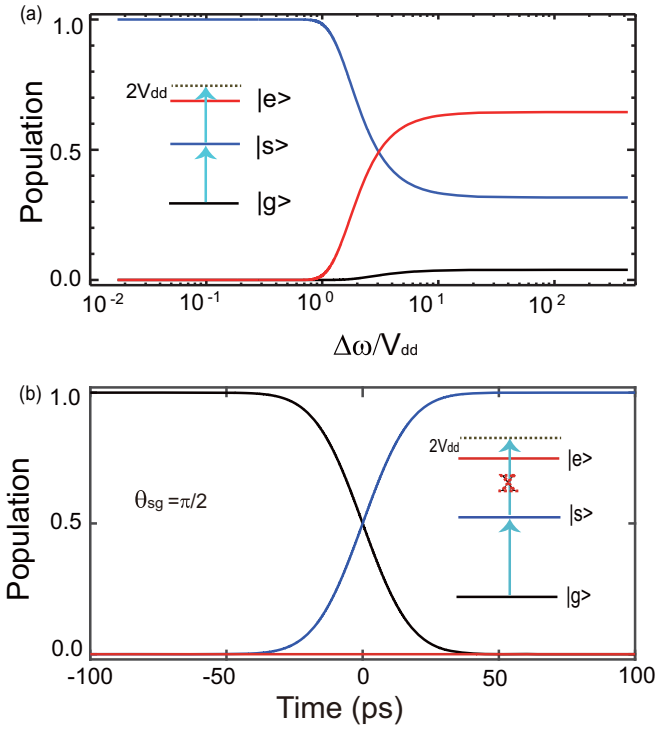

FIG. 2. (a) Final populations of $P_i(t_f)$ in states $|g\rangle$, $|s\rangle$, and $|e\rangle$ as a function of the bandwidth $\Delta\omega$ by using Gaussian laser pulses, and (b) the time-dependent population of the three states induced by using an extremely long pulse with bandwidth of $\Delta\omega = 0.02V_{dd}$, where V_{dd} denotes the strength of dipole-dipole interaction between atoms.

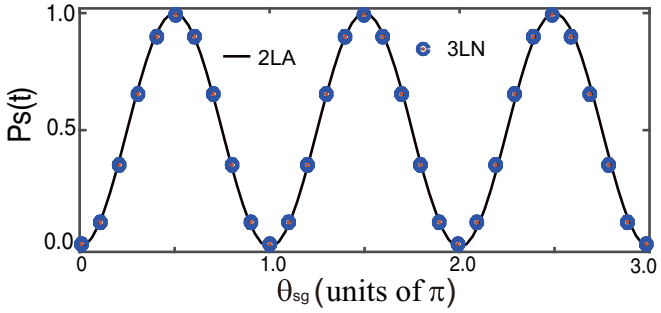

FIG. 3. The final population $P_s(t_f)$ as a function of $\theta_{sg}(t_f)$ by varying the value of ϑ from 0 to 6 for the laser pulse defined by Eq. (16) while fixing the bandwidth of the exciting pulse at $\Delta\omega = 0.02V_{dd}$. The black line denotes two-level analytical (2LA) simulation by using Eq. (12) at $\theta_{es}(t_f) = 0$, and the blue circles correspond to the three-level numerical (3LN) results by solving Eq. (3) with the three-level Hamiltonian defined by Eq. (4).

III. RESULTS AND DISCUSSION

To illustrate our method, two electronic levels $5S_{1/2}$ and $5P_{1/2}$ of individual rubidium-87 atoms are used to represent $|0\rangle$ and $|1\rangle$ of qubit with transition frequency $\omega_0 = 12578.95\ \mathrm{cm}^{-1}$ and transition dipole moment $\mu = 7.61$ Debye. We consider the dipole-dipole interaction of $V_{dd} = 12.35\ \mathrm{cm}^{-1}$, corresponding a case of $d = 100$ a.u. and $\alpha = \pi/2$. We employ a Gaussian laser laser pulse,

$$\mathcal{E}(t) = \sqrt{\frac{\pi}{2}}\frac{\vartheta}{\mu^d \tau} e^{\frac{-t^2}{2\tau^2}} \cos(\omega_c t), \tag{16}$$

to excite the trapped atoms. In our simulations, we take the initial time of $t_0 = -4\tau$ and the final time of $t_f = 4\tau$. By making Fourier transform of $\mathcal{E}(t)$ into the frequency domain, we can verify that the choice of such a pulse is able to satisfy the condition of $\theta_{sg} = \pi/2$ with $\vartheta = 1$ and $\omega_c = \omega_{sg}$ for an arbitrary duration of τ. Figure 2(a) shows the final populations in states $|g\rangle$, $|s\rangle$, and $|e\rangle$ as a function of the bandwidth $\Delta\omega$ (i.e.,$1/\tau$) with $\theta_{sg}(t_f) = \pi/2$. Due to $\theta_{es}(t_f) \neq 0$, the double excitation to state $|e\rangle$ plays roles in the regime of $\Delta\omega > V_{dd}$, whereas in the regime of $\Delta\omega \ll V_{dd}$ it is blocked, leading to the maximally entangled state $|s\rangle$. As an example, Fig. 2(b) shows the time-dependent populations of three states by using a pulse with $\Delta\omega = 0.02V_{dd}$ ($\tau = 22000$ fs). A fidelity of $P_s(t_f) > 0.9999$ is obtained while significantly suppressing the time-dependent population of the double-excitation state $|e\rangle$ to a very small value of $P_e(t) < 10^{-4}$. That is, the dipole-dipole interactions between single-excitation states prevent the further transitions from $|s\rangle$ to $|e\rangle$, and therefore the three-level system by Eq. (4) is reduced into an equivalent two-level system, in good agreement with the pulse area theorem by Eq. (12).

We further examine such a case of $\Delta\omega = 0.02V_{dd}$ by varying the values of ϑ. Figure 3 shows the final population $P_s(t_f)$ as a function of $\theta_{sg}(t_f)$ based on the two-level analytical (2LA) solution by using Eq. (12) and the three-level numerical (3LN) solution with the "exact" method by Eqs. (3) and (4) without using any Magnus-type expansion of U. We examine the pulse area $\theta_{sg}(t_f)$ from 0 to 3π, which corresponds to a variation of ϑ from 0 to 6 by Eq. (16). The population $P_s(t_f)$ in the entangled state $|s\rangle$ oscillates between 0 at the integer multiple of π and 1 at the half-integer multiple of π, in good agreement with the pulse area theorem of the two-level system. Thus, Rabi oscillations are exhibited, which are similar to the typical single-atom Rabi oscillations between the ground state $|0\rangle$ and the excited state $|1\rangle$, but here the ground state $|g\rangle$ couples to the Bell state $|s\rangle$ with an effective transition dipole moment $\mu^d = \sqrt{2}\mu$ and a blue-shifted transition frequency of $\omega_0 + V_{dd}$. We can also see that the 3LN simulations are consistent with the 2LA solution, indicating that the first leading term $S^{(1)}(t)$ can be used to describe the time-dependent unitary operator $U(t, t_0)$ at high precision. As a result, we are able to obtain an analytical solution for generating the maximally entangled Bell state. Note that the solution in Eq. (12) is general for an arbitrary time-dependent laser field. Although we perform the simulations in Figs. 2 and 3 by tuning the center frequency of ω_c to the resonance frequency ω_{sg}, the blockade of double excitation and Rabi oscillations within the two-level model can also be observed by using the pulses with ω_c at a single-excitation frequency ω_0 of individual atoms as well as other frequencies, as long as the pulsed fields satisfy the two conditions of $\theta_{sg}(t_f) = \pi/2$ and $\theta_{es}(t_f) = 0$.

We now perform the optimization to search for optimal laser pulses with the bandwidths of $\Delta\omega \geqslant V_{dd}$ while fixing the values of $\omega_c = \omega_{sg}$ and $\vartheta = 1$. We examine three different initial fields $\mathcal{E}(x_0, t)$ with $\Delta\omega \approx 4.0V_{dd}$ ($\tau = 100$ fs), $\Delta\omega \approx 1.7V_{dd}$ ($\tau = 250$ fs), and $\Delta\omega \approx 1.0V_{dd}$ ($\tau = 400$ fs), and then

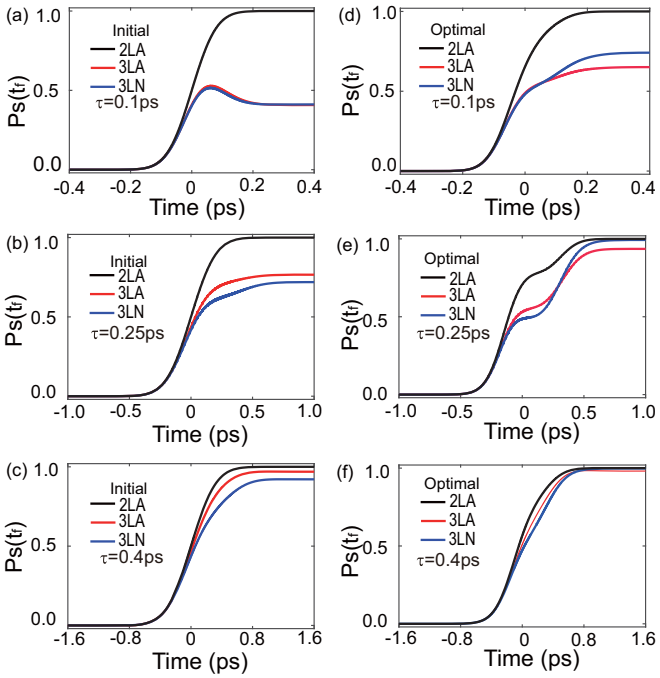

FIG. 4. The time-dependent populations of the state $|s\rangle$ for both three different initial fields (a)–(c) and the corresponding optimized fields (d)–(f). In each panel, the black line denotes the two-level analytical (2LA) results by using Eq. (12) while ignoring the level $|e\rangle$ in Fig. 1(d), the red line corresponds to the three-level analytical (3LA) results, and the blue line is the three-level numerical (3LN) results by solving Eq. (3) with the three-level Hamiltonian defined by Eq. (4).

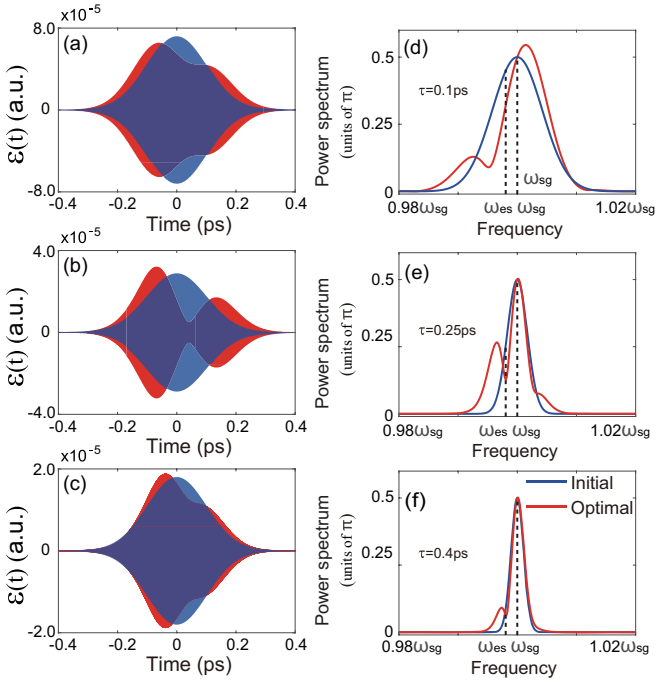

FIG. 5. (a)–(c) The initial fields (blue line) and the optimal fields (red line) used for Fig. 4, and (d)–(f) the corresponding spectral amplitude scaled by a factor of $\sqrt{2}\mu$.

optimize the laser pulse for each by using the algorithm of Eq. (15). For comparisons, Fig. 4 shows the time-dependent populations of the state $|s\rangle$ for initial and optimal fields based on the 2LA, the three-level analytical (3LA) and the 3LN simulations, respectively. The initial inputs in Figs. 4(a)–4(c) are able to generate the maximally entangled state $|s\rangle$ based on the 2LA model by ignoring the double excitation to state $|e\rangle$. However, the broad-bandwidth pulses open the transition to $|e\rangle$, destroying the two-level model. In addition, there is a difference between 3LA and 3LN simulations, which is slight for the case of $\Delta\omega \approx 4.0V_{dd}$ but becomes obvious for the cases of $\Delta\omega \approx 1.7V_{dd}$ and $\Delta\omega \approx 1.0V_{dd}$. Since the analytical solution in Eq. (12) only includes the first leading term $S^{(1)}(t)$ to denote the unitary operator $U(t, t_0)$, this difference indicates that the high order terms in Magnus expansion play roles.

The optimized pulses, as shown in Figs. 5(a)–5(c), are able to improve the fidelity of $|s\rangle$ with $P_s(t_f) = 0.7416$ for $\Delta\omega \approx 4.0V_{dd}$, $P_s(t_f) > 0.99$ for $\Delta\omega \approx 1.7V_{dd}$, and $P_s(t_f) > 0.999$ for $\Delta\omega \approx 1.0V_{dd}$ in Figs. 4 (d)–4(f), respectively. It is interesting to note that the bigger difference between 3LA and 3LN simulations observed in Figs. 4(a)–4(c), the higher fidelity of entangled state can be obtained in Figs. 4(d)–4(f). Figures 5(d)–5(f) plot the Fourier transforms of the initial inputs and the corresponding optimized fields scaled by a factor of $\sqrt{2}\mu$. The spectra are kept unchanged at ω_{sg} [i.e., $\theta_{sg}(t_f) = \pi/2$], whereas the optimized spectra at ω_{es} [i.e., $\theta_{es}(t_f)$] are decreased but not to zero. It implies that the optimization algorithm under the constraints is to search for optimal pulses by reducing the pulse area $\theta_{es}(t_f)$ while modulating the contributions of high-order terms of Magnus expansion to state $|e\rangle$. As can be seen from Figs. 5(b) and 5(c), the temporal shapes of the optimized pulses look simple and smooth, consisting of two time-delayed pulses, which could be designed in quantum coherent control experiments. However, the underlying control mechanism is different from the typical double-pulse coherent control schemes [52], which usually takes advantage of quantum interference between pulses. This pulse shaping approach is also different from the spectral-phase shaping techniques [43,53], which prolong the temporal shapes of the optimized fields. That is, the optimized fields exhibit three main features. First, the center frequency of the second pulse is shifted from the critical frequencies, i.e., ω_{sg}, ω_{es} of the system. Second, the optimized pulses in the present problem are found to reduce transitions to $|e\rangle$ by decreasing the value of $\theta_{es}(t_f)$. Third, the optimized fields are utilized to modulate the nonlinear transitions between states by the higher order terms of Magnus expansion. As a result, quantum state transfer to $|s\rangle$ is enhanced by suppressing the transfer to $|e\rangle$. To further gain an insight into the quantum dynamics of the system, Fig. 6 plots the time-dependent populations in three states $|g\rangle$, $|s\rangle$, and $|e\rangle$ driven by the initial pulses and Figs. 6(d)– 6(f) the optimized pulses. The population dynamics induced by the optimized pulses change as compared with that induced by the initial pulses, and the corresponding controlling schemes also vary from case to case. By decreasing the duration of the laser pulse, the quantum state transfer to state $|e\rangle$ induced by the initial pulses becomes more and more visible from Fig. 6(c) to Fig. 6(a). It exhibits a strong dependence of $P_e(t)$ on the bandwidth of the laser pulse. The optimized fields are capable of suppressing this transfer to $|e\rangle$ by using a

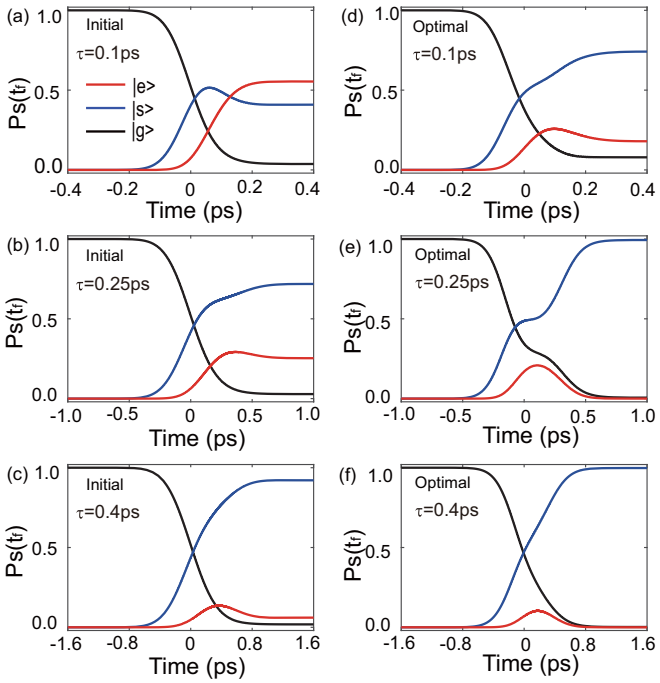

FIG. 6. The time-dependent populations in three states $|g\rangle$, $|s\rangle$, and $|e\rangle$ driven by (a)–(c) the initial pulses and (d)–(f) the optimized pulses in Fig. 5.

double-pulse controlling scheme, in which the second pulse not only transfers population to $|s\rangle$ but also suppresses the transfer to $|e\rangle$. As a result, a steplike behavior of population dynamics is visible in Fig. 6(d), and becomes more clear in Fig. 6(e), and then disappears in Fig. 6(f). Note that the optimized fields and the corresponding population dynamics will become more complex than those in Figs. 5 and 6 if we release the second and third constraints starting with an arbitrarily guess. The controlling schemes in Figs. 6(d)–6(f) also indicate that the population transfer dynamics induced by the optimized pulses is not an adidabatic process, because clearly visible populations appear in the excited state $|e\rangle$ in the presence of the laser pulses, whereas by using the adiabatic schemes the system can be adiabatically transferred from the initial state to the target state while suppressing the population transfer to the intermediate state. In addition, although a three-level system is used in our model, the optical transitions are also different from a typical stimulated Raman adiabatic passage (STIRAP) [54,55] in the three-level Λ system and adiabatic passage by light-induced potentials (APLIP) [56] with three electronic states of molecules in a ladder configuration.

Finally, we discuss the application of the present method to practical quantum systems. The use of the ultrafast laser pulse under strict constraints is still able to generate the Bell state beyond the two-level model. Usually, the optimal time control of quantum state transfer cannot be reached to its quantum speed limit in practice [57], due to bounds in the control strength, phase, and bandwidth. As can be seen from Fig. 4(a) the optimal field with a bandwidth of $\Delta\omega > 4.0V_{dd}$ only improves the fidelity of entangled state to a value of 0.7416. To that end, we have to keep in mind the fact that we use a two-level model to describe individual atoms by ignoring other levels. The choice of the bandwidth of ultrafast pulses in our system is limited by the level $5P_{3/2}$, which is only above $5P_{1/2}$ about $20V_{dd}$ in energy. Thus, the bandwidth of the optimized pulses is also expected to be far below this limit. Our method is able to search for optimal solutions under these strict constraints on both systems and control fields.

IV. CONCLUSION

We combined QOCT with theoretical analysis to show how to generate a maximally entangled state in a prototype quantum system of two identical neutral atoms interacting through Ising coupling. We reexamined the pulse area theorem to obtain an analytical wave function for describing the system within a three-level ladder system. We found that the three-level model can be reduced into an equivalent two-level model by interacting with a pulsed laser field in the extremely narrow bandwidth regime. It, in turn, provides an analytical approach to generate the perfect Bell state while exhibiting the dipole-dipole interaction blockade and Rabi oscillations. Since the ultrafast laser pulses break down the two-level model, we solved a highly constrained optimization problem to calculate an optimal control field. We imposed multiple constraints simultaneously to strictly fix the optimized pulses with no dc offset, a constant pulse area at resonant transition frequency, and a constant pulse fluence. By analyzing the results with three different level descriptions, we found that the constraints strongly limited the searching space to obtain the optimal solutions but resulted in simple and smooth solutions. We gained insights into the underlying control mechanism by using the optimized pulses. That is, the first-order term of Magnus expansion plays a leading role in the time-dependent unitary operator, whereas the higher-order terms play a role in eliminating the effect of other states. Our method presents a potentially useful approach to access all-optical control of quantum systems by shaping ultrafast laser pulses under multiple strict limitations. In principle, our method can also be applied to other quantum control problems and systems, e.g., consisting of a few spins or Rydberg atoms [58]. It is also interesting to examine our approach for a model of Ref. [46], in which the antisymmetric state $|a\rangle$ couples to other levels due to the spatial variation of the laser phase.

For practical applications, the spectral limitations of ultrafast laser pulses should be taken into account the optimization algorithm [37,38,40], and therefore it is an important extension of our multiple constraint QOCT methods in Ref. [42] to include the spectral constraints. A more direct approach is to search for the optimized fields by using the frequency-domain QOCT algorithm in line with the current ultrafast pulse shaping technique, which has been addressed recently in Ref. [43]. For the accuracy of the modeling system, the theoretical model can be further extended to include other levels excluded in the two-level approximation. In addition, the perturbations by noise and other experimental uncertainties may also affect the fidelity of generating maximally entangled state, which requires a design of optimal pulses robust against such uncertainties. Recently, we have demonstrated an efficient approach to search for optimal pulses to achieve robust control of quantum state transfer by using the frequency-domain QOCT algorithm [45].

ACKNOWLEDGMENTS

This work was supported in part by the National Natural Science Foundation of China (NSFC) under Grants No. 61803389, No. 11465009, and No. 11165009, and the Hunan Provincial Natural Science Foundation of China under Grant No. 2017JJ2272.

[1] R. P. Feynman, Int. J. Theo. Phys. **21**, 467 (1982).
[2] T. D. Ladd, F. Jelezko, R. Laflamme, Y. Nakamura, C. Monroe, and J. L. O'Brien, Nature (London) **464**, 45 (2010).
[3] J. Q. You and F. Nori, Nature (London) **474**, 589 (2011).
[4] M. H. Devoret and R. J. Schoelkopf, Science **339**, 1169 (2013).
[5] D. Loss and D. P. DiVincenzo, Phys. Rev. A **57**, 120 (1998).
[6] B. E. Kane, Nature (London) **393**, 133 (1998).
[7] J. I. Cirac and P. Zoller, Nature (London) **404**, 579 (2000).
[8] D. Kielpinski, C. Monroe, and D. J. Wineland, Nature (London) **417**, 709 (2002).
[9] I. Buluta, S. Ashhab, and F. Nori, Rep. Prog. Phys. **74**, 104401 (2011).
[10] D. Jaksch, J. I. Cirac, P. Zoller, S. L. Rolston, R. Côté, and M. D. Lukin, Phys. Rev. Lett. **85**, 2208 (2000).
[11] M. A. Nielsen and I. L. Chuang, *Quantum Computation and Quantum Information* (Cambridge University Press, Cambridge, 2000).
[12] R. Horodecki, P. Horodecki, M. Horodecki, and K. Horodecki, Rev. Mod. Phys. **81**, 865 (2009).
[13] J. Q. Liao, Y. Guo, H. S. Zeng, and L. M. Kuang, J. Phys. B: At. Mol. Opt. Phys. **39**, 4709 (2006).
[14] L. M. Kuang, Z. B. Chen, and J. W. Pan, Phys. Rev. A **76**, 052324 (2007).
[15] Y. Guo and L. M. Kuang, J. Phys. B: At. Mol. Opt. Phys. **40**, 3309 (2007).
[16] D. Stefanatos and E. Paspalakis, Opt. Lett. **43**, 3313 (2018).
[17] A. Gratsea, G. M. Nikolopoulos, and P. Lambropoulos, Phys. Rev. A **98**, 012304 (2018).
[18] P. Kurpiers, P. Magnard, T. Walter, B. Royer, M. Pechal, J. Heinsoo, Y. Salathé, A. Akin, S. Storz, J. C. Besse, S. Gasparinetti, A. Blais, and A. Wallraff, Nature (London) **558**, 264 (2018).
[19] M. Bock, P. Eich, S. Kucera, M. Kreis, A. Lenhard, C. Becher, and J. Eschner, Nat. Commun. **9**, 1998 (2018).
[20] S. Gómez, A. Mattar, I. Machuca, E. S. Gómez, D. Cavalcanti, O. J. Farías, A. Acín, and G. Lima, Phys. Rev. A **99**, 032108 (2019).
[21] S. L. Ma, X. K. Li, X. Y. Liu, J. K. Xie, and F. L. Li, Phys. Rev. A **99**, 042336 (2019).
[22] R. G. Unanyan, N. V. Vitanov, and K. Bergmann, Phys. Rev. Lett. **87**, 137902 (2001).
[23] Z. Eldredge, Z.-X. Gong, J. T. Young, A. H. Moosavian, M. Foss-Feig, and A. V. Gorshkov, Phys. Rev. Lett. **119**, 170503 (2017).
[24] A. Baksic, H. Ribeiro, and A. A. Clerk, Phys. Rev. Lett. **116**, 230503 (2016).
[25] R. de Vivie-Riedle and U. Troppmann, Chem. Rev. **107**, 5082 (2007).
[26] K. Hosaka, H. Shimada, H. Chiba, H. Katsuki, Y. Teranishi, Y. Ohtsuki, and K. Ohmori, Phys. Rev. Lett. **104**, 180501 (2010).
[27] J. D. Wong-Campos, S. A. Moses, K. G. Johnson, and C. Monroe, Phys. Rev. Lett. **119**, 230501 (2017).
[28] D. S. Weiss and M. Saffman, Physics Today **70**, 7, 44 (2017).
[29] T. Wilk, A. Gaëtan, C. Evellin, J. Wolters, Y. Miroshnychenko, P. Grangier, and A. Browaeys, Phys. Rev. Lett. **104**, 010502 (2010).
[30] H. Levine, A. Keesling, A. Omran, H. Bernien, S. Schwartz, A. S. Zibrov, M. Endres, M. Greiner, V. Vuletić, and M. D. Lukin, Phys. Rev. Lett. **121**, 123603 (2018).
[31] A. Browaeys, D. Barredo, and T. Lahaye, J. Phys. B: At. Mol. Opt. Phys. **49**, 152001 (2016).
[32] J. Werschnik and E. K. U. Gross, J. Phys. B: At. Mol. Opt. Phys. **40**, R175 (2007).
[33] C. Brif, R. Chakrabarti, and H. Rabitz, New J. Phys. **12**, 075008 (2010).
[34] S. J. Glaser, U. Boscain, T. Calarco, C. P. Koch, W. Köckenberger, R. Kosloff, I. Kuprov, B. Luy, S. Schirmer, T. Schulte-Herbrüggen, D. Sugny, and F. K. Wilhelm, Eur. Phys. J. D **69**, 279 (2015).
[35] A. Castro, J. Werschnik, and E. K. U. Gross, Phys. Rev. Lett. **109**, 153603 (2012).
[36] D. J. Egger and F. K. Wilhelm, Phys. Rev. Lett. **112**, 240503 (2014).
[37] C. Gollub, M. Kowalewski, and R. de Vivie-Riedle, Phys. Rev. Lett. **101**, 073002 (2008).
[38] P. von den Hoff, S. Thallmair, M. Kowalewski, R. Siemering, and R. de Vivie-Riedle, Phys. Chem. Chem. Phys. **14**, 14460 (2012).
[39] J. P. Palao, D. M. Reich, and C. P. Koch, Phys. Rev. A **88**, 053409 (2013).
[40] M. Lapert, R. Tehini, G. Turinici, and D. Sugny, Phys. Rev. A **79**, 063411 (2009).
[41] D. Sugny, S. Vranckx, M. Ndong, N. Vaeck, O. Atabek, and M. Desouter-Lecomte, Phys. Rev. A **90**, 053404 (2014).
[42] C.-C. Shu, T.-S. Ho, and H. Rabitz, Phys. Rev. A **93**, 053418 (2016).
[43] C.-C. Shu, T.-S. Ho, X. Xing, and H. Rabitz, Phys. Rev. A **93**, 033417 (2016).
[44] C.-C. Shu, D. Dong, I. R. Petersen, and N. E. Henriksen, Phys. Rev. A **95**, 033809 (2017).
[45] Y. Guo, D. Dong, and C.-C. Shu, Phys. Chem. Chem. Phys. **20**, 9498 (2018).
[46] S. Das, G. S. Agarwal, and M. O. Scully, Phys. Rev. Lett. **101**, 153601 (2008).
[47] K. Almutairi, R. Tanaś, and, Z. Ficek, Phys. Rev. A. **84**, 013831 (2011).
[48] D. Stefanatos and E. Paspalakis, Phys. Rev. A. **99**, 022327 (2019).
[49] S. Blanes, F. Casas, J. A. Oteo, and J. Ros, Phys. Rep. **470**, 151 (2009).
[50] G. Shchedrin, C. O'Brien, Y. Rostovtsev, and M. O. Scully, Phys. Rev. A **92**, 063815 (2015).

[51] S. M. Barnett and P. M. Radmore, *Methods in Theoretical Quantum Optics* (Clarendon Press, Oxford, 1997).
[52] K. Wilma, C.-C. Shu, U. Scherf, and R. Hildner, New J. Phys. **21**, 045001 (2019).
[53] K. Wilma, C.-C. Shu, U. Scherf, and R. Hildner, J. Am. Chem. Soc. **140**, 15329 (2018).
[54] N. V. Vitanov, A. A. Rangelov, B. W. Shore, and K. Bergmann, Rev. Mod. Phys. **89**, 015006 (2017).
[55] C.-C. Shu, J. Yu, K.-J. Yuan, W.-H. Hu, J. Yang, and S.-L. Cong, Phys. Rev. A **79**, 023418 (2009).
[56] B. M. Garraway and K.-A. Suominen, Phys. Rev. Lett. **80**, 932 (1998).
[57] M. Okuyama and M. Ohzeki, Phys. Rev. Lett. **120**, 070402 (2018).
[58] Qurrat-ul-Ain Gulfam and Z. Ficek, Phys. Rev. A **98**, 063824 (2018).